REFERENCES

[1] J. D. Cockroft, "The effect of curved boundaries on the distribution of electrical stress round conductors," *J. Inst. Elec. Eng.*, vol. 66, pp. 404–406, Apr. 1926.

[2] W. J. Getsinger, "Coupled rectangular bars between parallel plates," *IRE Trans. Microwave Theory Tech.*, vol. MTT-10, pp. 65–72, Jan. 1962.

[3] F. Bowman, *Introduction to Elliptic Functions with Applications.* New York: Dover, 1961, pp. 83–84.

[4] Harris Hancock, *Theory of Elliptic Functions.* New York: Dover, 1958.

Highly Efficient Calculation of Shielded Microstrip Structures in the Presence of Undercutting

VITTORIO RIZZOLI

Abstract—**Shielded microstrip transmission lines of a trapezoidal cross section such as resulting from the undercutting effect are analyzed by a highly efficient numerical technique, essentially consisting in a new formulation of the integral-equation approach. First, the method of electric images is used to change the conventional Fourier-series expansion of the Green's function into a fast-converging expression allowing the time required for computation to be reduced by more than two orders of magnitude. Then, the discretization of the Fredholm integral equation for the charge density on the strip surface is carried out by the Jacobi–Gauss integration formula, ensuring optimum accuracy for a given order of the solving matrix. In this way a very powerful tool for microstrip analysis and design is obtained, combining generality of application and excellent numerical performance.**

I. INTRODUCTION

SEVERAL METHODS are currently available [1, pp. 67–95] for computing the quasi-TEM properties of microstrip transmission lines, each having particular advantages and drawbacks that make it most suitable for selected applications. In the commonly encountered case of a system of thin strips enclosed by a rectangular metal shield, the variational method (such as described in [2], [3]) is unexcelled, both from the point of view of memory storage and CPU time. However, this method is not directly applicable when thick strips must be dealt with, unless by approximate assumptions that are supported by intuition but not rigorously justified [1, p. 83]. One possibility for solving the thick-strip problem is the use of finite-difference methods [4], [5], but these are usually too slow for design applications when realistic strip thicknesses (i.e., a few micrometers) are considered, involving an extremely large number of mesh points. This is particularly true when the effects of small changes of the microstrip cross-sectional shape are to be investigated, such as for the trapezoidal configurations resulting form undercutting [6]. In these cases, the method of solution to be preferred is the integral-equation method [1, p. 89], requiring direct manipulation of the Green's function for the rectangular inhomogeneous region enclosed by the shield.

Now, though an expression for the Green's function is readily obtained in rectangular geometry via Fourier-series expansion [7], these series converge far too slowly to be useful for design purposes when dealing with realistic strip geometries, as will be discussed later on. However, making use of the theory of electric images, the Fourier expansion can be changed into a rapidly converging series, allowing the computer time required for each evaluation of the Green's function to be reduced by at least two orders of magnitude. The generation of this fast-converging expression will be described in the next section.

In Section III it will be shown that this expression together with a new formulation of the integral-equation method provides a very powerful tool for microstrip analysis and design, combining the generality of the integral-equation approach with a numerical performance comparable with that obtained from the variational method. Finally, an example of the influence of undercutting on the electrical parameters of a shielded microstripline will be given in Section IV.

II. COMPUTATION OF THE GREEN'S FUNCTION

The cross section of the rectangular region to be considered is shown in Fig. 1 together with the relevant geometrical dimensions. For typical alumina microstrips we have

Manuscript received November 8, 1977; revised May 16, 1978. This work was partially sponsored by the Italian National Research Council (CNR).

The author is with the Istituto di Elettronica, University of Bologna, Villa Griffone, Pontecchio Marconi, Bologna, Italy.

0018-9480/79/0200-0150$00.75 ©1979 IEEE

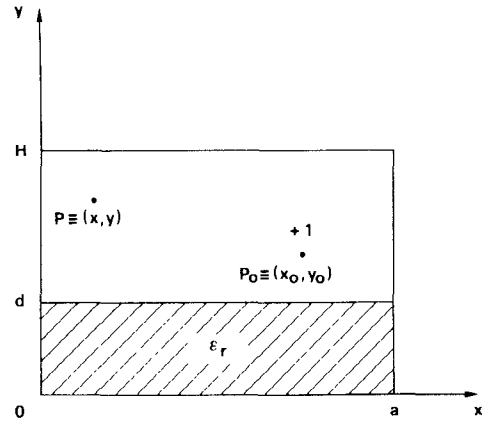

Fig. 1. Inhomogeneous rectangular region for which the Green's function has to be found.

$d=0.635$ mm, while the order of magnitude of a and H is one to a few centimeters.

Now let a unit charge be located at $P_0\equiv(x_0,y_0)$, $y_0 \geq d$. Making use of a Fourier-series expansion with respect to the x coordinate [7] the potential at $P\equiv(x,y)$, $y \geq y_0$ (i.e., the Green's function for the rectangular region) can be expressed as

$$G(P,P_0;\epsilon_r)=\sum_{n=1}^{\infty} F_n(y,y_0;\epsilon_r)\sin(C_n x)\sin(C_n x_0) \qquad (1)$$

where

$$C_n=\frac{n\pi}{a}$$

and

$$F_n(y,y_0;\epsilon_r)=\frac{2}{n\pi\epsilon_0}\sinh\{C_n(H-y)\}\frac{\cosh\{C_n(y_0-d)\}}{\cosh\{C_n(H-d)\}}\cdot\frac{\epsilon_r\tanh\{C_n(y_0-d)\}+\tanh(C_n d)}{\epsilon_r\tanh\{C_n(H-d)\}+\tanh(C_n d)}. \qquad (2)$$

For $y<y_0$ we still can make use of (1) and (2) due to the reciprocity theorem $G(P,P_0)=G(P_0,P)$. The relative dielectric constant ϵ_r has been explicitly put into evidence in (1) for later convenience. Note that for microstrip applications both y and y_0 are not greater than $d+t$, where t is the strip thickness (typically of the order of a few micrometers).

From (2), the following asymptotic form can be readily obtained for the coefficient $F_n(y,y_0;\epsilon_r)$:

$$\frac{\exp\{-C_n(y-y_0)\}}{n\pi\epsilon_0}\left[1+\exp\{-2C_n(y_0-d)\}\right]\cdot\frac{\epsilon_r\tanh\{C_n(y_0-d)\}+1}{\epsilon_r+1}. \qquad (3)$$

To write (3), only the exponential terms that for increasing n decay slower than $\exp\{-(2n\pi d/a)\}$ have been retained, while the remaining ones have been set to zero. Note that some of these terms may reduce to constants depending on the particular values of y and y_0.

Equation (3) shows that in the worst case (i.e., for $y=y_0$) the decay of $|F_n|$ with increasing n is essentially of the form $1/n$, which means that the convergence of the series (1) in extremely slow. This clearly appears from Fig. 2 where a typical convergence plot for the series (1) is reported. This plot refers to the geometry defined by (30) (see Section IV) and is drawn for $y=y_0$ and $|P-P_0|=20$ μm. It shows the dependence of the quantity $\Sigma(N)/\Sigma(\infty)$, where $\Sigma(N)$ is the sum of the first N terms of (1), against the number of added terms N. In typical cases, about 10^4 to 10^5 terms may be needed to get 10^{-3} to 10^{-4} relative accuracy on the sum, depending on the particular values of P and P_0. Thus the computation of microstrip structures making use of (1) is extremely demanding in terms of computer time.

To understand how a rapidly converging expression can be derived from (1), let us now recall the concept of partial image of an electric charge with respect to an air–dielectric interface. If there were no rectangular shield and the boundary conditions on the electric potential were reduced to the discontinuity of the dielectric constant occurring at $y=d$, then an exact expression for the Green's function at $y \geq d$ would be obtained by superimposing the free-space potentials of the actual charge, located at P_0, and its partial image located at $P_{0i}\equiv(x_0,2d-y_0)$.

The strength of the latter is given by

$$r=-\frac{\epsilon_r-1}{\epsilon_r+1}. \qquad (4)$$

Now turning back to the shielded microstrip problem, by analogy with the open-boundary case, we can presume that a major contribution to the Green's function be represented by the potential of the actual charge plus its partial image, both computed in the presence of the shield but assuming a homogeneous dielectric. This quantity can be expressed as

$$G(P,P_0;1)+rG(P,P_{0i};1). \qquad (5)$$

The contribution (5) may be explicitly put into evidence by adding (5) to and subtracting it from (1), thus obtaining

$$G(P,P_0;\epsilon_r)=G(P,P_0;1)+rG(P,P_{0i};1)+\sum_{n=1}^{\infty}K_n(y,y_0)\sin(C_n x)\sin(C_n x_0) \qquad (6)$$

where

$$K_n(y,y_0)=F_n(y,y_0;\epsilon_r)-\{F_n(y,y_0;1)+rF_n(y,2d-y_0;1)\}=r\frac{\exp\{-C_n(y-y_0)\}}{n\pi\epsilon_0}\cdot\frac{1-\exp\{-2C_n(H-y)\}}{1-\exp\{-2C_n H\}}\cdot\frac{1-\exp\{-2C_n y_0\}+r[\exp\{-2C_n(y_0-d)\}-\exp\{-2C_n d\}]}{1-\exp\{-2C_n H\}+r[\exp\{-2C_n(H-d)\}-\exp\{-2C_n d\}]}\cdot[\exp\{-2C_n d\}-\exp\{-2C_n(H-d)\}]. \qquad (7)$$

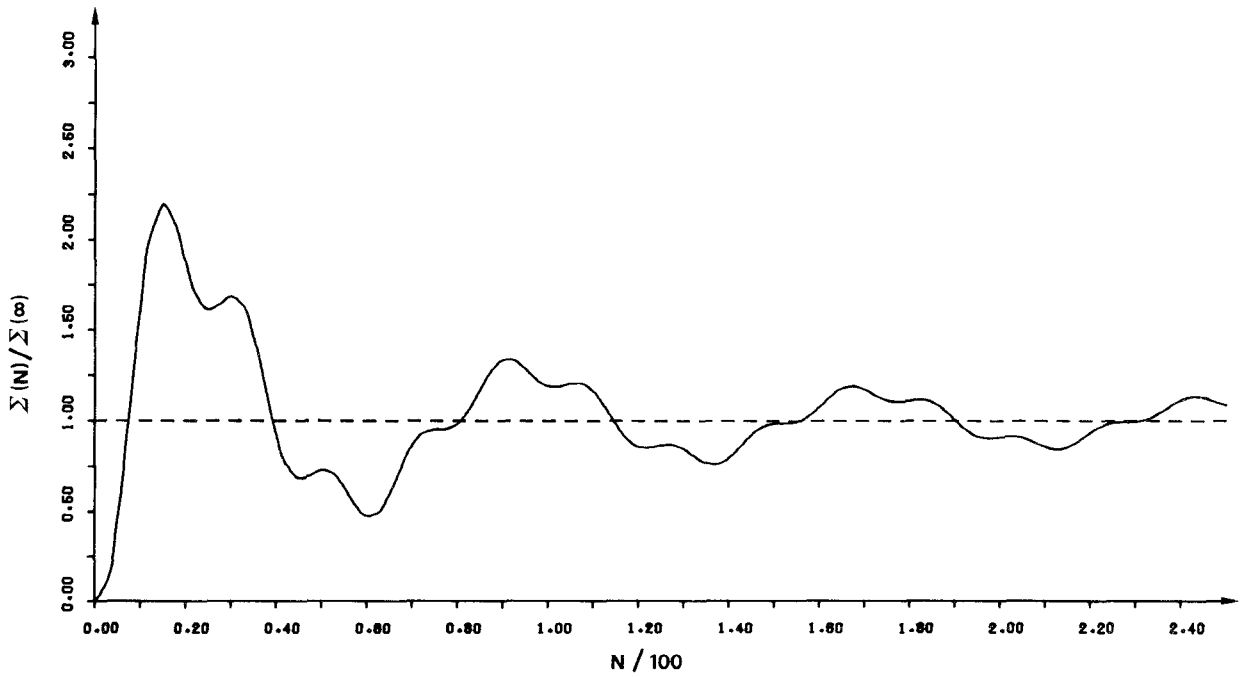

Fig. 2. Convergence plot for the Fourier-series expansion of the Green's function.

Since usually $H-d \gg d$, from (7) it is seen that $|K_n|$ has essentially the same rate of decay as $(1/n)\cdot \exp\{-(2n\pi d/a)\}$. As a consequence, the last term on the right-hand side of (6) is a fast-converging series provided that the ratio d/a be large enough. For a fixed substrate thickness this means that the outer shield should be relatively narrow to ensure good convergence of the series, but this is not a very stringent requirement for microstrip applications, since the effects of the shield are known to be negligible when it is 5 to 10 times as wide as the center strip conductor. As an example for the same geometry as referred to in Fig. 2 we have $d/a \simeq 0.084$ (see (30) in Section IV); in this case only 18 terms are needed to get a relative accuracy of 10^{-3}, while adding 37 terms reduces the error to 10^{-7}. This is a fairly good performance as compared to that obtained from (1). A substantially similar behavior can be observed over the whole range of geometries involved by practically significant microstrip problems.

By means of (6) the problem is thus reduced to finding an efficient expression for the Green's function of the homogeneous rectangular region. Again, this problem can be solved by the method of images.

First consider a homogeneous region between two infinite ground planes at $y = 0, y = H$. The Green's function for this case is known [8] and can be expressed as the following:

$$g_0(P,P_0)=\frac{1}{4\pi\epsilon_0}\ln\frac{\sinh^2\frac{\pi(x-x_0)}{2H}+\sin^2\frac{\pi(y+y_0)}{2H}}{\sinh^2\frac{\pi(x-x_0)}{2H}+\sin^2\frac{\pi(y-y_0)}{2H}}. \tag{8}$$

To allow for the remaining boundary conditions, that is, the metal walls at $x=0$, a, the original unit charge at (x_0,y_0) is replaced by an infinite array of charges of alternate signs (and equal magnitudes) located at $(2na \pm x_0,y_0)$, $-\infty < n < \infty$. Summing all of the contributions to the potential at (x,y) we obtain

$$G(P,P_0;1)=\sum_{n=\infty}^{\infty}\left[\, g_0(x,y,2na+x_0,y_0) - g_0(x,y,2na-x_0,y_0)\right] \tag{9}$$

which is the required expression. Note that the nth term of (9) (i.e., the quantity in square brackets) has an exponential decay with increasing $|n|$ (for $|n|$ large) of the form

$$\exp\left\{-2|n|\frac{\pi a}{H}\right\}. \tag{10}$$

For commonly encountered microstrip configurations a and H have the same order of magnitude so that (9) converges much faster than the third term on the right-hand side of (6). Thus the CPU time required to compute (6) is essentially determined by the latter.

A convergence plot of the expression (6) is given in Fig. 3 for the same geometry as referred to in Fig. 2. For convenience, the quantity to be plotted is now defined as

$$10000\left\{\frac{\Sigma(N)}{\Sigma(\infty)}-1\right\} \tag{11}$$

where $\Sigma(N)$ is the sum of (5) plus the first N terms of the infinite summation appearing in (6). A comparison between Figs. 2 and 3 clearly shows the dramatic improvement in numerical efficiency that is obtained by using (6) and (9) instead of (1). In fact, the computer time needed

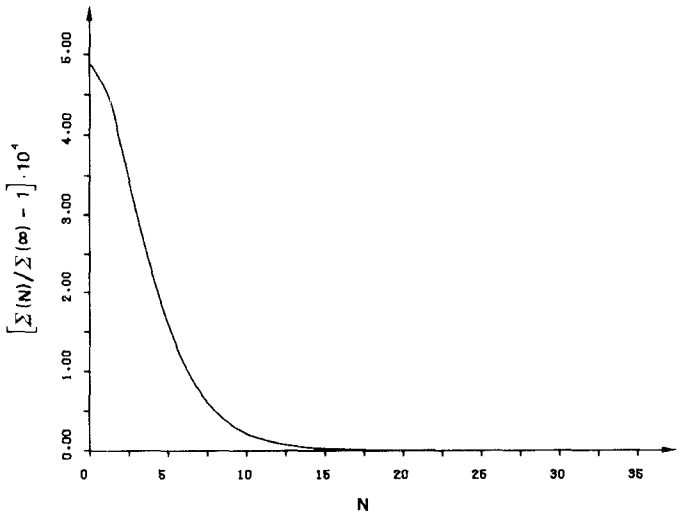

Fig. 3. Convergence plot for the fast-converging expression of the Green's function.

to find the Green's function by (1) with a relative accuracy of 10^{-3} is typically 250 times as large as that required to get the same result from (6) with a relative error as low as 10^{-11}.

An interesting point appearing from Fig. 3 is that for the case considered here (5) actually represents a major contribution to the Green's function as suggested by the intuitive argument presented before. In fact, neglecting at all the infinite summation in (6) would lead to an error smaller than 0.05 percent. Thus for this case we can write

$$G(P,P_0;\epsilon_r)\simeq G(P,P_0;1)+rG(P,P_{0i};1). \tag{12}$$

Further investigation has shown that the error involved in (12) is a rapidly increasing function of $|P-P_0|$ but remains less than about 0.5 percent for $|P-P_0|<0.1$ mm for $d=0.635$ mm and $\epsilon_r\simeq 10$. In all such cases, (12) can be used to calculate the Green's function, thus further reducing the computation time by a factor of about 20. Note that this is by no means a trivial point, since many microstrip applications of practical interest involve the use of strip conductors definitely narrower than 0.1 mm (e.g., the 3-dB interdigital coupler).

A final remark concerns the singularity of the Green's function at $P=P_0$. First let $y_0>d$. In this case by inspection of (6) and (9), it is found that the singularity is confined to the quantity $g_0(P,P_0)$ appearing in the first term on the right-hand side of (6). For later convenience, the expression (8) for $g_0(P,P_0)$ is now rewritten in the form

$$g_0(P,P_0)=\frac{1}{4\pi\epsilon_0}\ln\left[\sinh^2\frac{\pi(x-x_0)}{2H}+\sin^2\frac{\pi(y-y_0)}{2H}\right]+\frac{1}{4\pi\epsilon_0}\ln\frac{\left\{\frac{\pi(x-x_0)}{2H}\right\}^2+\left\{\frac{\pi(y-y_0)}{2H}\right\}^2}{\sinh^2\frac{\pi(x-x_0)}{2H}+\sin^2\frac{\pi(y-y_0)}{2H}}+S_0(P,P_0) \tag{13}$$

where

$$S_0(P,P_0)=-\frac{1}{4\pi\epsilon_0}\ln\left[\left\{\frac{\pi(x-x_0)}{2H}\right\}^2+\left\{\frac{\pi(y-y_0)}{2H}\right\}^2\right]. \tag{14}$$

Note that the first and second terms on the right-hand side of (13) are regular at $P=P_0$, so that the singularity is reduced to the simple logarithmic form (14). The Green's function may then be expressed as

$$G(P,P_0;\epsilon_r)=G_R(P,P_0;\epsilon_r)+S(P,P_0) \tag{15}$$

where G_R is regular at $P=P_0$ and $S=S_0$. An expression for G_R is readily obtained from (6), (9), and (13).

In the case $y_0=d$ the actual charge and its partial image are superimposed ($P_0\equiv P_{0i}$), so that (5) reduces to

$$(1+r)G(P,P_0;1). \tag{16}$$

Thus (15) is still valid with the new definition

$$S(P,P_0)=(1+r)S_0(P,P_0). \tag{17}$$

The expression (15) of the Green's function is particulary convenient in view of the application of the integral-equation method, since it allows the singular terms to be directly handled in closed form.

III. Application of the Integral-Equation Method

The rapidly converging expression of the Green's function that was derived in the previous section will now be used together with a new formulation of the integral-equation method to compute the electrical parameters of the shielded microstrip structure in Fig. 4. To approximately account for the effects of undercutting, the cross section of the strip conductor is assumed to be of trapezoidal shape [6]; the degree of undercutting is related to the values of the angles ϕ_1, ϕ_2.

Let the center conductor of the structure be held at a constant potential of 1 V. Then a Fredholm integral equation for the unknown charge density on the strip surface is

$$1=\oint G(P,P_0;\epsilon_r)\rho(P_0)\,ds_0 \tag{18}$$

where P, P_0 are points on the strip contour, and ds_0 is the differential line length around P_0.

To change (18) into a matrix equation, the surface of the strip conductor is usually divided into a number of subsections and a uniform or linear charge density distribution is assumed on each section [7]. In this paper we will make use of the well-known properties of the integration formulas of Gaussian type [9] in order to optimize the discretization process, that is, to obtain optimum accuracy for a given order of the solving matrix.

As a first point note that the charge density $\rho(P_0)$ has a singularity at each corner of the integration path. From simple static considerations [10] it is found that the behavior of the charge density in the vicinity of each singular point depends on the angle between the two intersection conductors in the way summarized in Table I.

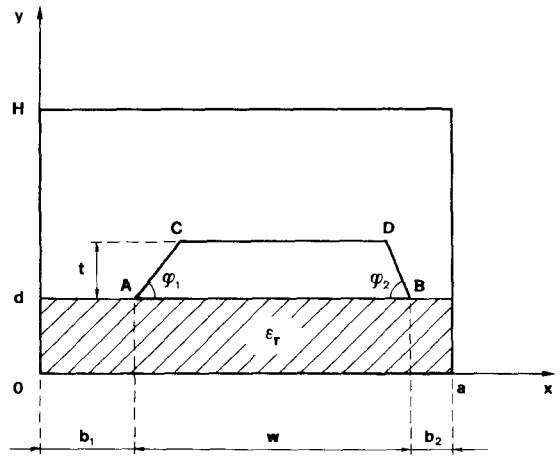

Fig. 4. Cross section of shielded microstrip line in the presence of undercutting.

TABLE I
BEHAVIOR OF THE CHARGE DENSITY IN THE VICINITY OF EACH SINGULAR POINT ON THE COUNTOUR OF INTEGRATION

Corner	Behavior of $\rho(P_0)$
A	$\lvert P_0 - A\rvert^{\frac{\phi_1 - \pi}{2\pi - \phi_1}}$
B	$\lvert P_0 - B\rvert^{\frac{\phi_2 - \pi}{2\pi - \phi_2}}$
C	$\lvert P_0 - C\rvert^{\frac{-\phi_1}{\pi + \phi_1}}$
D	$\lvert P_0 - D\rvert^{\frac{-\phi_2}{\pi + \phi_2}}$

The integral on the right-hand side of (18) can now be decomposed into the sum of four contributions of the form

$$\int_{-T/2}^{T/2} G(P,P_0;\epsilon_r)\rho(P_0)\,ds_0 \tag{19}$$

arising from the four sides of the trapezoidal conducting boundary. In (19) it is understood that the coordinates of the point P_0 are related to the variable of integration s_0 by

$$x_0 = X + \frac{1}{2}\left(1+\frac{2s_0}{T}\right)\cos\theta$$
$$y_0 = Y + \frac{1}{2}\left(1+\frac{2s_0}{T}\right)\sin\theta \tag{20}$$

where X, Y, θ are constants whose values can be obtained from Fig. 1 by inspection, and T is the length of the side under consideration. If the charge density is now given the expression

$$\rho(P_0) = \left(\frac{T}{2}-s_0\right)^{\alpha}\left(\frac{T}{2}+s_0\right)^{\beta} R(P_0) = W(s_0)R(P_0) \tag{21}$$

and α, β are chosen according to Table I so that the function $W(s_0)$ accounts for the singularity of the integrand at $s_0 = \pm T/2$, then $R(P_0)$ turns out to be regular and finite over the closed interval $-T/2 \leqslant s_0 \leqslant T/2$. Thus if P *does not* belong to the integration path we can compute (19) by the Jacobi–Gauss integration formula [9]

$$\int_{-T/2}^{T/2} W(s_0)G(P,P_0;\epsilon_r)R(P_0)\,ds_0 \simeq \sum_{i=1}^{m} H_i G(P,P_i;\epsilon_r)R_i \tag{22}$$

where m is an integer. The point P_i appearing in (22) is obtained from (20) by letting $2s_0/T = x_i$, where x_i is the ith zero of the polynomial

$$V_m(x) = (1-x)^{-\alpha}(1+x)^{-\beta}\frac{d^m}{dx^m}\{(1-x)^{\alpha+m}(1+x)^{\beta+m}\}. \tag{23}$$

The ith weight has the expression

$$H_i = T^{\alpha+\beta+1}\frac{\Gamma(m+\alpha+1)\Gamma(m+\beta+1)}{(\Gamma(m+\alpha+\beta+1))} \cdot \frac{2^{2m}m!}{(1-x_i^2)\{V_m'(x_i)\}^2} \tag{24}$$

(Γ = Euler's function), and $R_i = R(P_i)$.

If P belongs to the integration path, i.e., is obtained from (20) for $s_0 = s(-T/2 < s < T/2)$, then the integrand of (19) has a logarithmic singularity at $s_0 = s$. In this case we make use of (15) and write

$$\begin{aligned}\int_{-T/2}^{T/2} W(s_0)G(P,P_0;\epsilon_r)R(P_0)\,ds_0 &= \int_{-T/2}^{T/2} W(s_0)G_R(P,P_0;\epsilon_r)R(P_0)\,ds_0 \\ &+ \int_{-T/2}^{T/2} W(s_0)S(P,P_0)\left[R(P_0) - R(P)\frac{W(s)}{W(s_0)}\right]ds_0 \\ &+ W(s)R(P)\int_{-T/2}^{T/2} S(P,P_0)\,ds_0.\end{aligned} \tag{25}$$

The first two terms on the right-hand side of (25) have a regular integrand for $-T/2 < s_0 < T/2$ (in particular, the integrand of the second term vanishes at $s_0 = s$) and can again be approximated by the Jacobi–Gauss formula; the third term can be exactly calculated by means of (14). Letting $P = P_j$ in (25) yields

$$\int_{-T/2}^{T/2} G(P_j,P_0;\epsilon_r)\rho(P_0)\,ds_0 \simeq \sum_{i=1}^{m} f_{ji}R_i \tag{26}$$

where

$$f_{ji} = H_i G(P_j,P_i;\epsilon_r) \qquad (i \neq j) \tag{27}$$

and

$$f_{JJ} = H_J G_R(P_J, P_J; \epsilon_r) - \sum_{\substack{i=1 \\ i \neq J}}^{m} H_i S(P_J, P_i) \left(\frac{1-x_J}{1-x_i}\right)^{\alpha} \left(\frac{1+x_J}{1+x_i}\right)^{\beta} + \frac{K}{2\pi\epsilon_0} \left(\frac{T}{2}\right)^{\alpha+\beta+1} (1-x_J)^{\alpha}(1+x_J)^{\beta} \cdot \left[2 - (1-x_J) \ln \frac{\pi T(1-x_J)}{4H} - (1+x_J) \ln \frac{\pi T(1+x_J)}{4H}\right]. \quad (28)$$

According to the previous section, in (28) we have $K = 1 + r$ if the side being considered is AB, $K = 1$, otherwise.

Finally, the contribution to the capacitance per unit length of the microstripline, arising from the side under consideration, may be put into the form

$$\int_{-T/2}^{T/2} \rho(P_0) ds_0 \simeq \sum_{i=1}^{m} H_i R_i. \quad (29)$$

At this stage the way the integral equation (18) is discretized has become evident. For each side of the conducting boundary a set of discrete points P_i and a corresponding set of scalar unknowns R_i is chosen according to the above discussion. The electrostatic potential at any of these points, say P_j, is then expressed as the sum of three integrals of the form (22) and one integral of the form (25), and equated to 1. Repeating the same procedure for all the values of j yields a matrix equation for the R_i's. The off-diagonal terms of the system matrix are given by (27), while the diagonal terms have the form (28). Once the system has been solved by matrix inversion the capacitance can be found by adding four contributions of the form (29). To speed up the computations, once the values of ϕ_1 and ϕ_2 (usually $\phi_1 = \phi_2$) have been established in relation to a given technological process, the abscissas and weights of the Gaussian integration for selected values of m are calculated once and for all, and then stored in the computer memory as DATA items.

IV. Numerical Results

The performance of the above approach will now be discussed by comparison with the variational method [1], [2] for the special case of a thin microstrip ($t = 0$, $\phi_1 = \phi_2 = 0$). In this case the Jacobi–Gauss formula reduces to a standard Chebyshev–Gauss integration [9] since $\alpha = \beta = -1/2$.

Let us consider a microstripline having the following geometrical parameters (see Fig. 4):

$$a = 7.6 \text{ mm} \qquad d = 0.635 \text{ mm}$$
$$H = 10 \text{ mm} \qquad \epsilon_r = 10 \quad (30)$$
$$b_1 = 7.5 \text{ mm}$$
$$w = 75\ \mu\text{m} \qquad b_2 = 25\ \mu\text{m}. \quad (31)$$

While (30) can be considered typical, (31) define a highly asymmetrical cross section, i.e., an extremely narrow strip very close to the right electric wall. This choice is made intentionally, in order to give a clear account of the performance of the method in a very ill-conditioned case. Note that such dimensions are not unrealistic for present-day MIC applications; for instance, the geometry described by (31) could be associated with one of the odd modes propagating in a microstrip 3-dB interdigitated coupler [11].

Now let M be the total number of scalar unknowns used to solve the problem. The characteristic impedance Z_c of the microstripline was computed for several values of M ranging from 3 up to 200. Since no appreciable change was found between $Z_c(100)$ and $Z_c(200)$, the latter was assumed as the "true value" of the impedance, i.e., $Z_c(200) \simeq Z_c(\infty)$. The percentage error $100\ \{Z_c(M)/Z_c(200) - 1\}$ is plotted against M in Fig. 5, where the error resulting from the application of the variational method [3] is also reported. This error is in excess (+0.61 percent) because the impedance was obtained from a lower-bound calculation of the capacitance. Note that the variational formulation of [3] had to be used for the present case, since the method of [2], based on the computation of a symmetrical cell, is inadequate for the highly asymmetrical geometry considered here. Fig. 5 shows that the accuracy of the solution is rapidly increasing with increasing M; for $M > 20$ the error is lower than 1 percent, while an accuracy better than 3 percent (which is usually enough for all practical purposes) is obtained for M as low as 10. From the figure it can be seen that the integral-equation method becomes more accurate than the variational approach for M larger than about 24.

The CPU time required to compute the characteristic impedance is plotted against M in Fig. 6. Curves a and b refer to the use of the expressions (6) and (12) for the Green's function, respectively. The latter yields practically the same accuracy as the former since in the present case $w < 0.1$ mm. The unit used to measure time is the computation time required to obtain the variational solution. Fig. 6 shows that the integral-equation approach yields the same accuracy as the variational method (see the vertical line in the figure) in less than 4 time units by using (6) and slightly more than 1.5 unit by (12). Further note that if a 3-percent error is tolerated ($M = 10$), the computation can be carried out in 0.6 time units by (6) and less than 0.3 time units by (12).

The above considerations clearly show that the particular formulation of the integral-equation method described in this paper is very efficient from the numerical point of view, its performance being comparable with that obtained from the variational method. Furthermore, an excellent tradeoff between accuracy and time requirements can be obtained, which makes the method attractive for design applications. The situation is even more favorable for better conditioned geometries than the one considered above, such as symmetric microstrip lines.

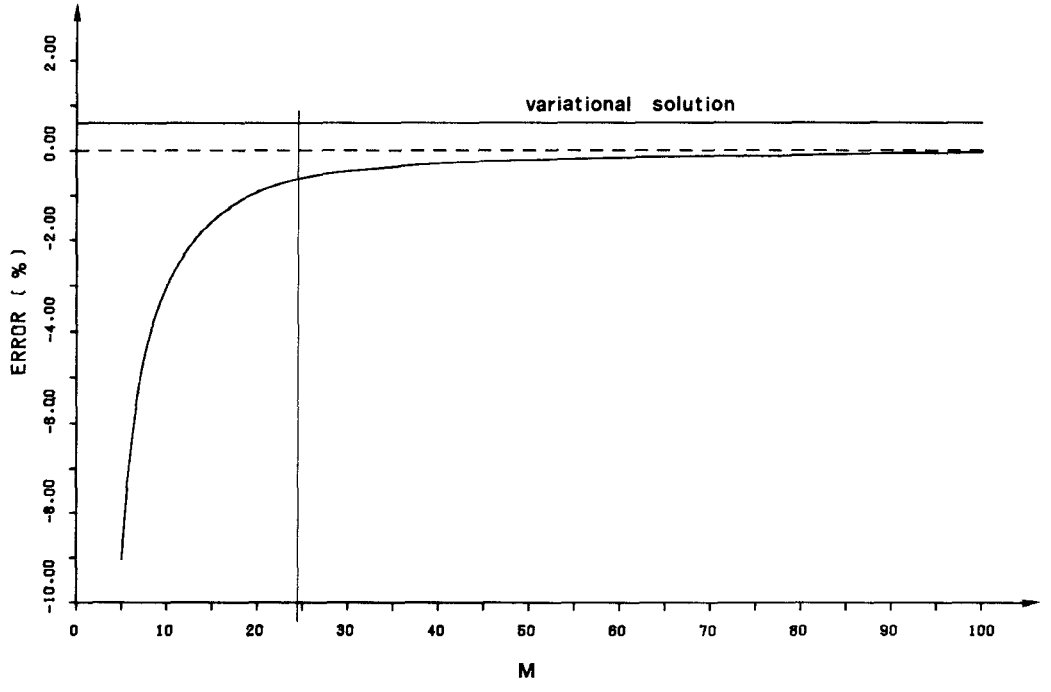

Fig. 5. Accuracy of the integral-equation solution verus order of the matrix to be inverted (the vertical line corresponds to the value of M for which the same accuracy is obtained from the integral-equation approach and the variational method).

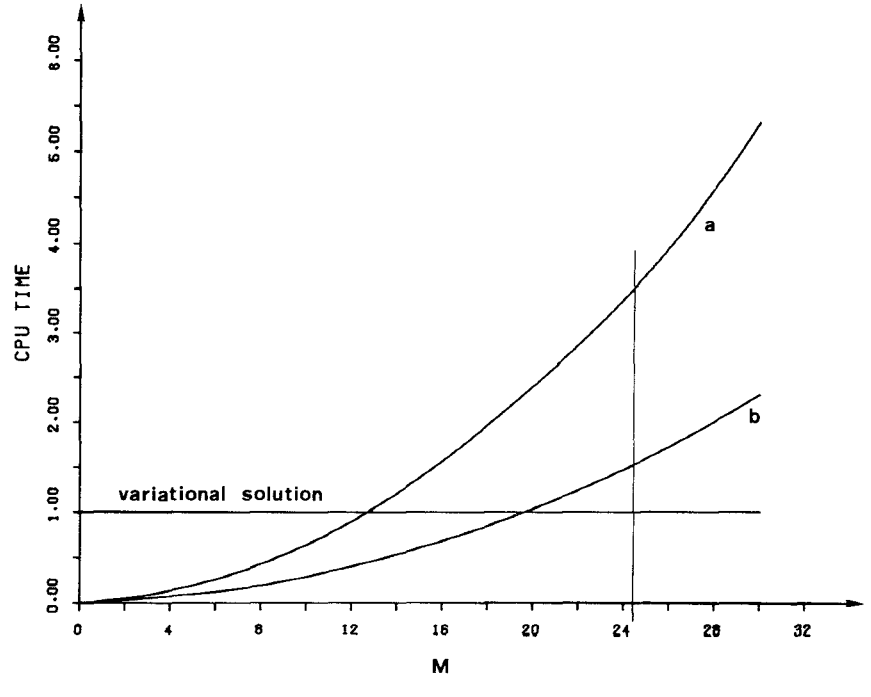

Fig. 6. CPU time required by the integral-equation solution versus order of the matrix to be inverted. Curve *a* corresponds to the use of (6) for the Green's functions, curve *b* to the use of (12).

An illustrative application to thick microstrips is shown in Fig. 7, where the characteristic impedance of the same microstrip as considered before is plotted against strip thickness t in the cases of: *a*) no undercutting ($\phi_1=\phi_2=90°$); b) "normal" undercutting ($\phi_1=\phi_2=45°$); and *c*) "heavy" undercutting ($\phi_1=\phi_2=30°$). The range of t values considered encompasses both the cases of thin- and thick-film circuitry [12].

A few indications of technical interest can be drawn from Fig. 7. It is well known [1, pp. 32–34] that the technique used to define patterns in metal layers strongly influences the resulting cross-sectional shape of the strips.

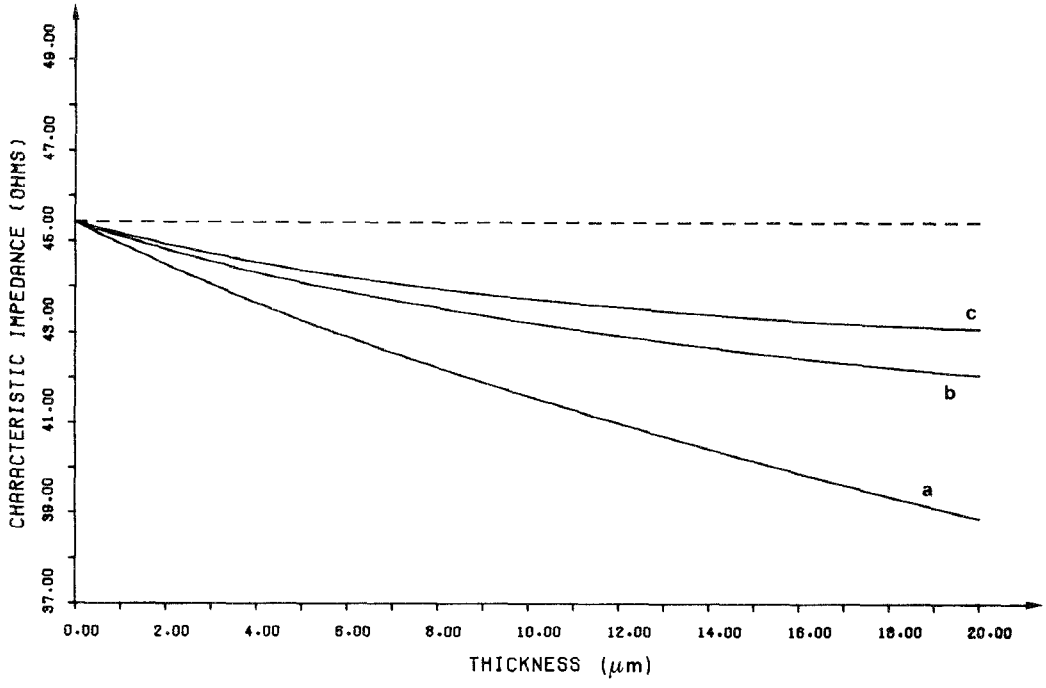

Fig. 7. Dependence of microstrip characteristic impedance on strip thickness with: *a*—no undercutting ($\phi_1 = \phi_2 = 90°$); *b*—"normal" undercutting ($\phi_1 = \phi_2 = 45°$); *c*—"heavy" undercutting ($\phi_1 = \phi_2 = 30°$).

If a very thin seed metal layer is etched and then plated to increase thickness and lower conductor losses, then a cross section with practically no undercutting will result. In this case, the change of the electrical properties of the microstrip lines with respect to the ideal thin-strip case may be quite large as shown by Fig. 7 (curve *a*), especially in the case of tightly coupled strips. On the other hand, if a thick metal layer is etched to directly obtain the final circuit, then "normal": undercutting will typically occur. The electrical behavior of the microstrip in this case is definitely closer to that of the zero-thickness strip, as can be seen from the figure (curve *b*). This is found to be true to an even greater extent in the case of "heavy" undercutting (curve *c*).

A final remark concerns the behavior of fired-film (or thick-film) circuits. The cross-sectional shapes of the conductors built by this technique [1, p. 44] are well approximated by the trapezoidal shape of Fig. 4 with ϕ_1 and ϕ_2 of the order of 30°, corresponding to the "heavy" undercutting case considered above for thin-film circuits. Thus it is not surprising that conventional microstrip calculations based on the zero-thickness assumption may be used [12] to accurately design thick-film devices.

The above considerations have limited significance from the design standpoint since they only provide qualitative information. In order to thoroughly account for the effects of undercutting one should determine how the zero-thickness design data for practical devices must be modified when dealing with microstrip lines of trapezoidal shape. Such problems are currently being investigated and the results will be reported elsewhere.

References

[1] L. Young and H. Sobol, Eds., *Advances in Microwaves*, vol. 8. New York: Academic Press, 1974.

[2] J. I. Smith, "The even- and odd-mode capacitance parameters for coupled lines in suspended substrate," *IEEE Trans. Microwave Theory Tech.*, vol. MTT-19, pp. 424–431, May 1971.

[3] V. Rizzoli, "A unified variational solution to microstrip array problems," *IEEE Trans. Microwave Theory Tech.*, vol. MTT-23, pp. 223–234, Feb. 1975.

[4] *Advances in Microwaves*, vol. 2, L. Young, Ed. New York: Academic Press, 1967, pp. 327–390.

[5] A. Wexler, "Computation of electromagnetic fields," *IEEE Trans. Microwave Theory Tech.*, vol. MTT-17, pp. 416–440, Aug. 1969.

[6] L. I. Maissel and R. Glang, *Handbook of Thin-Film Technology*. New York: McGraw-Hill, 1970, pp. 7.44–7.45.

[7] E. Yamashita and K. Atsuki, "Analysis of thick-strip transmission lines," *IEEE Trans. Microwave Theory Tech.*, vol. MTT-19, pp. 120–122, Jan. 1971.

[8] L. V. Bewley, *Two-Dimensional Fields in Electrical Engineering*. New York: Dover, 1963, pp. 157–160.

[9] F. B. Hildebrand, *Introduction to Numerical Analysis*. New York: Mc Graw-Hill, 1956.

[10] S. Ramo, J. R. Whinnery, and T. Van Duzer, *Fields and Waves in Communication Electronics*. New York: Wiley, 1967, pp. 180–182.

[11] V. Rizzoli and A. Lipparini, "The design of interdigitated couplers for MIC applications," *IEEE Trans. Microwave Theory Tech.*, vol. MTT-26, pp. 7–15, Jan. 1978.

[12] D. C. Rickard, "Thick-film MIC components in the range 10-20 GHz," in *Proc. 6th European Microwave Conf.* (Rome, Italy, Sept. 1976), pp. 687–691.